Electric Field Reversals Resulting from Voltage Waveform Tailoring in Ar/O_2 Capacitively Coupled Plasmas Sustained in Asymmetric Systems

Florian Krüger[1], Hyunjae Lee[2], Sang Ki Nam[2] and Mark J. Kushner[1,3]

[1] Electrical Engineering and Computer Science Department, University of Michigan, 1301 Beal Ave., Ann Arbor, MI 48109-2122 USA

[2] Mechatronics R&D Center, Samsung Electronics Co., Ltd., 1-1 Samsungjeonja-ro, Hwaseong-si, Gyeonggi-do 18448, South Korea

[3] Author to whom correspondence should be addressed.

Email: fkrueger@umich.edu, hj0928.lee@samsung.com, sangki.j.nam@samsung.com, mjkush@umich.edu

Abstract:

The etching of nanometer scale high-aspect-ratio (HAR) features into dielectric materials in low pressure radio frequency excited plasmas is often accompanied by charge accumulation inside the features which can slow etching rates and produce distortions such as twisting. The intra feature charging is at least partially produced by differences in electron and ion energy and angular distributions (EADs). Positive ions, accelerated to high energies having narrow angular spreads by the sheath electric field, can penetrate deeply into HAR features. Electrons typically arrive at the wafer with nearly thermal and isotropic distributions and do not penetrate deeply into HAR features. These disparities lead to differential charging of the inside of the feature, which can lead to reductions in etch rate and feature distortion due to ion deflection. With increasing aspect ratio of features, charging challenges are expected to continue for the foreseeable future. In this work, the use of tailored voltage waveforms in geometrically asymmetric capacitively coupled plasmas sustained in Ar/O_2 at 40 mTorr was computationally investigated with the goal of shaping the EAD of electrons incident onto the substrate to address differential charging. The tailored waveform consisted of a sinusoidal wave and its higher harmonics with a fundamental frequency of 1 MHz. We found that electric field reversals in the sheath and presheath can occur during the anodic portion of the cycle. The electric field reversal increases the energy and decreases the angular spread of electrons incident onto the substrate. The magnitude of the electric field reversal can be controlled by the phase angle of the even harmonics and the gas composition. Due to its electronegative nature, increasing mole fractions of O_2 impedes electron transport to the surface which further increases the electric field reversal.

Keywords: Voltage Waveform Tailoring, Plasma Etching, High Aspect Ratio Etching, Electric Field Reversal, Plasma Sheath

I. Introduction

Plasma etching of dielectrics such as SiO_2 and Si_3N_4 is an integral process in nearly all micro- and nanometer scale electronics fabrication.[1] The etching of high aspect ratio (HAR) features is becoming an increasingly critical process due to the development of 3-dimensional structures such as 3D-NAND memory which requires contact holes through more than 256 alternating layers of SiO_2 and Si_3N_4 with a total aspect ratio of up to 100.[2,3] Plasma etching of HAR features requires ions having highly anisotropic velocity distributions incident onto the wafer which arrive with a near normal angle. This anisotropy is a consequence of acceleration of positive ions by the electric field in the sheath bounding the wafer. The majority of HAR etching of dielectrics is performed in capacitively coupled plasmas (CCPs) sustained in fluorocarbon gas mixtures, typically using multiple radio frequency (RF) power supplies. [4,5] Typical operating conditions are tens of mTorr gas pressure with hundreds of watts to many kW power deposition over a 30 cm diameter wafer. [4] These conditions produce ion fluxes to the wafer of 10^{15}-10^{16} $cm^{-2}s^{-1}$.[6] To enable these ion fluxes (or hot neutral fluxes after ion scattering from sidewalls) to reach the bottom of HAR features with sufficient energy and narrow angular distribution to continue the etch, applied voltages to the substrate are as high as 5 kV while endeavoring to minimize ion collisions inside the sheath.[7]

The electric field in the sheath above the wafer points towards the wafer surface during the majority of the RF cycle, accelerating positive ions to high energies and narrow angular spreads. This same electric field confines electrons to the bulk plasma. It is only during a small fraction of the RF cycle at which time the sheath collapses that electron flux from the bulk plasma reaches the wafer. The highly anisotropic, near normal, high energy ions can penetrate deeply into HAR features whereas the electrons typically have nearly thermal and angularly broad distributions onto the wafer.[1] When etching dielectric (or low conductivity materials), these conditions result in the lower echelons of the feature being charged positively and the upper echelons being charged negatively.[8,9] This differential charging generates electric field components within the feature.[8–10] The intra-feature electric fields can deviate ion trajectories from the vertical which can lead to undesired consequences including a reduction of the ion flux at the bottom of the feature [11], and profile distortion such as notching, twisting and bowing [8–15]

Several remedies have been investigated to minimize differential charging, including op-

eration with ever higher ion energies to minimize the effects of ion deflection. However, this approach must overcome several challenges. Increasing the ion energy increases the power density at the wafer surface, leading to wafer heating which, unchecked, can stress the thermal budget of the process.[4] In HVM (high volume manufacturing) additional wafer cooling is applied. While this strategy has been very successful it adds technological complexity to the etch system and is ultimately subject to diminishing returns due to the limited heat transport of coolants and the wafer itself.

Another challenge is that the sheath thickness is a function of the sheath voltage and, by extension, is a function of the CCP power. If the source power and plasma density are relatively constant, increasing the incident ion energy by increasing the applied bias voltage will ultimately lead to a thicker and more collisional sheath. The more collisional sheath will produce a lower energy and broader angular distribution of the incident ion flux. The higher ion energies are also incident onto the photoresist or other hard masking materials, resulting in higher physical sputtering rates, which then decrease the selectivity of the dielectric etch with respect to the mask. Maintaining high selectivity is critical during the typically long etch times required for HAR features.[16]

Another approach to mediating differential charging is to produce enhanced fluxes of negative charge carriers into the feature. Once such method utilizes power-pulsing to generate an ion-ion plasma during the inter-pulse period. Acceleration of negative ions into the feature during the interpulse period helps alleviate positive charging.[17] This technique is challenged by the difficulty of sustaining a thin sheath during the low-plasma density afterglow, and so the ion acceleration through the sheath is collisional. Another technique utilizes a negative DC bias on the top electrode to generate an electron-beam-like flux of electrons into the feature [1].

In a CCP of the type used for plasma etching of dielectrics in microelectronics fabrication (pressures of tens of mTorr, frequencies of 1 – 100 MHz), the net charged flux to dielectric surfaces in contact with the plasma must sum to zero over the RF cycle in the steady state,

$$\int_0^T \left(\Gamma_e(t) - \Gamma_i(t)\right) dt = 0 \tag{1}$$

where, T is the RF period. $\Gamma_e(t)$ and $\Gamma_i(t)$ are the time dependent fluxes to the surface of electrons and positive ions, acknowledging that the flux of negative ions is negligible in the absence of pulsing. The electric field in the sheath and presheath usually point towards surfaces to accel-

erate ions out of the plasma and confine electrons. It is only during a small portion of the anodic part of the RF cycle that the sheath voltage decreases sufficiently to enable electrons to reach the substrate. These electrons arrive at the substrate with largely thermal, isotropic velocity distributions. Voltage waveform tailoring (VWT) is technique that is able to generate directional (anisotropic), high energy electron fluxes onto the substrate through promoting an electric field reversal (EFR) in the presheath above the substrate [18,19]. EFR refers to the electric field in the presheath pointing into the plasma, as opposed to pointing towards the surface. In VWT, a non-sinusoidal voltage is applied to the substrate, typically using several harmonics of a fundamental frequency.[18] EFR in the presheath ultimately results from the requirement that the time average of positive and negative fluxes to the substrate must balance. Only during the sheath collapse during the anodic part of the cycle are electrons able to diffuse to the surface. Under certain conditions, this diffusive electron transport may not be sufficient to satisfy the local charge balance. This lack of ability for diffusive electrons to reach the surface in sufficient numbers may be due to short sheath collapse times, thick sheaths, or magnetically or collisionally hindered transport. For these conditions, negative space charge in the presheath produces an EFR, which slows the transport of ions and speeds the transport of electrons towards the wafer. Electric field reversal has been observed computationally as well as experimentally.[18–21]

With its ability to produce anisotropic energy and angular distributions (EADs) of electrons onto the substrate which can penetrate deeply into HAR features, EFR produced by voltage waveform tailoring has been proposed as a (partial) remedy for charging inside HAR features.[18] In principle, if the flux of positive ions and negative electrons that penetrate deeply into features can be balanced, the detrimental effects of intra-feature charging can be minimized. Since the production of EFR requires manipulating the sheath potential during the RF cycle, the ion EADs are also affected, and so independent control of the EADs of both electrons and ions is a challenge.

The dynamics of VWT, and EFR in particular, are sensitive to the geometry of the plasma reactor and the electronegativity of the plasma. (Electronegativity refers to the ratio of negative ions to electrons. Highly electronegative plasmas have a large ratio of negative ions to electrons, while the RF cycle averaged plasma potential and floating potential are still positive.) For example, one of the features of VWT is the electrical asymmetry effect (EAE) in which the DC bias in a symmetric CCP can be controlled by the amplitude and phase of the harmonics used in

the bias waveform.[22–26] The plasma reactors used in HVM are typically geometrically asymmetric and produce a negative DC bias on the substrate on this basis alone. The VWT produced EAE then competes with or adds to the geometrically produced DC bias. This competition lead to an increase or decrease of the total DC bias, based on the polarity of the electrically induced asymmetry.[27] Electronegative plasmas further complicate the VWT produced EAE and EFR as space charge is maintained by far less mobile negative ions compared to electrons.[28,29]

In this paper we discuss results from a computational investigation of electric field reversal in electronegative CCPs sustained in Ar/O_2 mixtures in a plasma reactor similar to those used in HVM. In these simulations, the power deposition is held constant as frequency content is varied to acknowledge that in HVM, power (and not voltage) is usually what is controlled in HAR etching. The consequences of EFR on the EADs of ions and electrons onto the wafer surface are discussed. We found that the consequences of VWT are not limited to electron dynamics but also affect the EADs of ions mainly through the electrical asymmetry effect and the resulting change in the DC self-bias. The observed electric field reversal is almost entirely due to the inertia limited lack of electron conduction current and the decrease in sheath collapse time.

The computational platform used in this investigation, the Hybrid Plasma Equipment Model (HPEM) and the reactor conditions are discussed in Sec. II. The outcome of the investigation for the Ar-only base case is discussed in Sec. III with a focus on the influence of the phase angle φ as of the harmonic components of the waveform. In Sec. IV the influence on EFR of added oxygen, an electronegative species, to the gas mixture is discussed. Concluding remarks are in Sec. V.

II. Description of the Model

This investigation was performed using the Hybrid Plasma Equipment Model (HPEM), which is described in detail in Ref. [30]. In short, the HPEM is a 2-dimensional plasma hydrodynamics model which resolves plasma phenomena in a time-slicing approach. Different physics regimes are addressed in various modules that are coupled by exchanging physical quantities – electric and magnetic fields, densities, rate coefficients. The major modules used in this work are the Fluid Kinetics-Poisson Module (FKPM), the Electron Energy Transport Module (EETM), and the Plasma Chemistry Monte Carlo Module (PCMCM). In the FKPM, the continuity, mo-

mentum, and energy equations of the heavy particles are solved coincidently with Poisson's equation to provide heavy particle densities and electrostatic potential. In the EETM, the electron energy distributions (EEDs) are obtained using a kinetic, Monte Carlo based approach based on the space and phase resolved electric fields produced in the FKPM. In the EETM the energy and angular distribution (EAD) of electrons striking the substrate are recorded. Using the EEDs in the bulk plasma, electron transport and rate coefficients are obtained which are transferred to the other modules. After the plasma reaches a quasi-steady state the PCMCM, using Monte Carlo techniques, tracks the trajectories of ions and reactive neutral species. EADs of these species are recorded impinging onto the wafer. The reaction mechanism used for pure Ar plasmas is the same as that described in Ref. [31]. The mechanism for Ar/O_2 plasmas is a subset of that described in Ref. [32] which involves only Ar and O containing species. The mechanism for reactions between only O, O_2 and its excited and ion species is described in Ref. [33]. To decrease computational cost, excited states for O and O_2 were lumped into a single state.

A schematic of the cylindrically symmetric CCP reactor used in this investigation is shown in Fig 1. a) The reactor, modeled after multi-frequency CCPs used in in industrial etch applications, consists of two parallel plate electrodes with a diameter of 300 mm separated by a 2.8 cm gap. The top electrode also serves as a showerhead gas inlet. A 0.7 mm thick silicon wafer is mounted on the bottom electrode. A focus ring made of silicon and quartz to improve discharge uniformity surrounds the wafer. The dielectric constants of these components are $\varepsilon/\varepsilon_0 = 4$ for the outer quartz ring and $\varepsilon/\varepsilon_0 = 11.8$ for the Si ring. While the conductivity of the quartz is negligible, that of the Si wafer is 0.05/Ω-cm. The feedstock gas is a mixture of Ar and O_2 flowing at 500 sccm through the top electrode, with oxygen fractions of 0 to 50%. The reactor pressure is held constant at 40 mTorr at the location of the pressure sensor near the pump port. This is accomplished by throttling the rate of pumping. Secondary electron emission due to ion bombardment of surfaces is included with a coefficient of 0.15.

The wafer is naturally included in the self-consistent electric potential and current calculations by specifying its permittivity and conductivity, whose values are adjusted during execution of the model to accurately represent the actual thickness of the wafer. The conductivity of the wafer is large enough that the voltage drop across the wafer is only a few volts, and does not meaningfully affect the DC bias.

A general electric circuit diagram is shown in Fig 1b. The VWT power supply is con-

nected to the bottom electrode through a blocking capacitor C_B of 500 nF. In principle, in the quasi-steady state, the DC bias should be independent of the value of the blocking capacitor provided that the RC time constant of the plasma-capacitor series impedance is large compared to transients in current. The capacitance used here is a balance of there being an acceptably short charging time and long enough RC time constant so that there is little variation in the DC bias during the RF cycle. It may appear in the reactor schematic that the high frequency electrode is touching a grounded metal. Computationally, a zero-conductivity dielectric lies between the two metal materials. As a result, only displacement current flows between the metals that are separated by what appears to be a perfect capacitor. This is analogous to a dark-space shield. Averaged over a radio frequency cycle, there is no net power transfer nor net current passing between the two metals.

To maintain a relatively constant plasma density, 100 W of power is coupled into the discharge through the top electrode using a sinusoidal voltage V_{hf} with a frequency of 80 MHz. To control the dynamics of charged particles impinging on the wafer surface, a customized voltage waveform, $V(t)$, is applied to the bottom electrode. The waveform consists of a fundamental sine wave with a frequency f_0 = 1 MHz and 4 consecutive higher harmonics:

$$V(t) = V_0 \sum_{i=1}^{N} \frac{N-k+1}{N(N+k)} \cos(2k\pi f_0 t + k\pi\varphi_k) \tag{2}$$

Here, V_0 is the total applied voltage amplitude, k is the harmonic order, N is the total number of frequencies, and the relative phase shift of each harmonic frequency k is φ_k. In this work the number of harmonics is N = 5, and the consequences of VWT are studied by varying the phase shift of the even harmonics φ for k = 2, 4. The power coupled through the bottom electrode was held constant at 1 kW by adjusting V_0.

III. The Ar Base Case

The DC self-bias, V_{dc}, is a major factor governing charged particle dynamics in the plasma sheath. In conventional CCPs, the DC bias is a function of the applied voltage, reactor geometry and gas composition (especially electronegativity) [22,29]. The DC bias is also a function of the shape of the applied waveform through the generation of the electrical asymmetry effect [34–36]. Given these dependencies, the DC self-bias can be expressed as

$$V_{dc} = -\frac{V_{\max} + \varepsilon V_{\min}}{1+\varepsilon}, \tag{3}$$

where $V_{\max}$ and $V_{\min}$ are the maximum and minimum of the applied voltage. ε is the discharge symmetry parameter given by

$$\varepsilon = \left(\frac{A_p}{A_g}\right)^2 \frac{\bar{n}_{sp}}{\bar{n}_{sg}} \frac{I_{sg}}{I_{sp}}, \tag{4}$$

where the areas of the powered and ground electrodes are A_p and A_g and the mean ion densities at the sheaths at the powered and grounded surfaces are $\bar{n}_{sp}$ and $\bar{n}_{sg}$. I_{sp} and I_{sg} are the sheath integrals, described in prior publications on the origin of the EAE [23]. In short, the sheath integrals are dimensionless quantities that depend only on the normalized profile of the sheath charge density. This formulation does not specifically account for the presence of a second powered electrode. However, due to the higher frequency and lower power, the voltage amplitude applied to the top electrode is much smaller than that applied to the lower electrode, and sinusoidal voltages alone do not induce an EAE. For example, for the argon only, 40 mTorr base case with φ = 0°, the amplitude of the high frequency voltage, V_{hf}, on the top electrode to deliver 100 W is 47.4 V. The amplitude of the low frequency voltage, V_0, to deliver 1 kW is 1296 V.

V_{hf} and V_0 are shown in Fig. 2a as a function of the phase angle φ. The voltage waveforms for these cases are shown in Fig. 3d for phase shifts of φ = 0°, 45°, 90°, 135° and 180°. The high frequency power is constant at 100 W. Since the phase shift only applies to the tailored waveform on the bottom electrode and the plasma density remains fairly constant, V_{hf} also remains relatively constant for all φ, varying by less than 10%. Even with the low frequency power being constant at 1 kW, due to the changes to the electron dynamics in the sheath region, there is some variation in V_0, increasing from 1296 V to 1650 V or about 27%.

The DC self-bias as a function of the phase angle φ is shown in Fig. 2b for the argon base case conditions. The decrease in the magnitude of the DC self-biases (less negative) with increasing phase angle φ can be directly attributed to the EAE. At φ = 0° with $|V_{\max}| > |V_{\min}|$ (see Fig. 3d) the electrical asymmetry of the applied voltage is at its maximum, and the contribution of the EAE to the DC bias is most negative. The asymmetry is zero when φ = 90° with $|V_{\max}| = |V_{\min}|$ (see Fig. 3d) where the contribution of the EAE to the dc bias is also zero. The asymmetry is at its minimum at φ = 180° with $|V_{\max}| < |V_{\min}|$ (see Fig. 3d), at which point the con-

tribution of the EAE to the DC bias is most positive.

The axial components of the electric field between the two electrodes, $E_z(z, t)$, radially averaged across the wafer, are shown in Figs. 3a for phase shifts of $\varphi = 0°$, 45°, 90°, 135° and 180°. The electric fields are plotted as a function of time during a single 1 MHz cycle. The dotted line in the images is the $E_z(z, t) = 0$ contour. The respective voltage waveforms are shown in Fig 3d.

In plasmas which do not have EFR, $E_z(z, t)$ in the sheath at the bottom electrode will point towards the electrode at all times, which corresponds to a negative value of E_z in these images. However, even with pure argon, there can be an EFR at the peak of the positive excursion of the applied voltage waveform. With $\varphi = 0°$ the EFR occurs during the sheath collapse at around 0.5 μs when the applied voltage is at its maximum positive value and a positive electric field component (pointing in +z direction) is present. This EFR results, in part, from the short duration of the positive voltage excursion of the waveform. During more than 80% of the RF cycle, the applied voltage is negative, with there being less than 20% of the RF cycle being amenable to electron collection. Given that the electrons are mostly thermal, diffusion alone would not provide sufficient current to the wafer to balance the ion current during this short period. An additional drift component is required, which for electrons requires a net electric field pointing upwards (positively), away from the electrode. The reversal in the electric field provides additional electron acceleration to overcome the confining potential and inertial effects to enable the charge and current balance conditions. The generation of the EFR is a natural outcome of the calculation due to solution of Poisson's equation and the charge transport equations.

The densities of Ar^+ and electrons as a function of height averaged across the wafer are shown in the Figs. 3b and 3c as a function of time and for different values of φ. Maximum ion densities increase from 2.8×10^{10} cm^{-3} for $\varphi = 0°$ to 6.9×10^{10} cm^{-3} for $\varphi = 180°$. Recall that the power deposition at both frequencies is being held constant. With a decrease in the magnitude of V_{dc} (less negative) with increasing φ (see Fig. 2), less fractional power is dissipated by ion acceleration through the sheath. The response of the system is to increase V_o and V_{hf} (the latter being a small increase) to increase plasma density to maintain a constant power. In spite of its large mass, there is a small response of the Ar^+ density profile to the sheath dynamics, with ions being accelerated into the lower sheath during the local maxima of the cathodic portion of the low frequency RF cycle. Ions are accelerated into the upper sheath during the local maxima of the an-

odic cycle. These responses are afforded, in part, by the low fundamental frequency of 1 MHz. Such responses would not be expected, for example, at 13.56 MHz. In contrast, the spatial distribution of electron density in the sheaths is strongly modulated during both the RF cycle and with different values of φ. Electrons are excluded from the lower sheath during the local maxima of the cathodic portion of the low frequency RF cycle and excluded from the upper sheath during local maxima of the anodic portion of the cycle.

A phase angle of $\varphi = 0°$ produces the "peak" waveform (Fig. 3d, left-most sub-image) which approximates a delta function for higher harmonic orders ($N \rightarrow \infty$). As such, it creates the shortest period of sheath collapse having the largest time derivate in electric field (dE_z/dt), both of which favor EFR. With larger phase angles, this abrupt sheath collapse becomes more gradual and longer, providing electrons with more time to diffuse to the surface, which reduces the need for EFR to balance current. With $\varphi = 180°$, the voltage waveform resembles the "valley" waveform (Fig. 3d, right-most sub-image) which results in a plasma sheath that is at its minimum voltage and width most of the time – the opposite of the $\varphi = 0$ waveform. This change in φ from 0 to 180° produces a decrease of the EFR, with its elimination for $\varphi = 180°$. A portion of this reduction (and eventual elimination) of the EFR with increasing phase angle is due to the decrease of the magnitude of the DC self-bias (less negative) which reduces electron repulsion from the sheath. Although the instantaneous electron diffusion flux from the bulk plasma may appear to be sufficient to balance current, that flux is actually limited by the ambipolar-like electric fields in the presheath and by the finite time required for electrons to cross the sheath. The secondary electrons emitted from the surface generate a net positive current into the wafer when the sheath expands, increasing the requirements to balance current by the bulk electrons during sheath collapse.

The EADs of electrons incident onto the wafer for the pure argon plasma for different phase angles φ are shown in Fig. 4a. The mean electron energy and angle of incidence are shown in Fig. 4b as a function of phase angle. The trends in the maximum strength of the EFR translate to the EADs. The electron temperature in the bulk plasma is 3.1- 3.3 eV, which is approximately the temperature of the electrons incident onto the wafer for $\varphi = 180°$ which has the minimum EFR. This similarity, including the broad angular distribution, indicates that the electrons are simply diffusing into the sheath with there being little drift component. With decreasing φ, conditions which increase the EFR, there is an increase in directional electron acceleration

onto the wafer. With decreasing phase angle the EADs increase in energy while becoming more narrow in angle. As the phase angle decreases from 180° to 0°, the mean energy of electrons incident onto the wafer increases from 7.1 eV to 17.3 eV, while the mean angle of incidence decreases from 26.8° to 15.1°. These results suggest that high fluxes of directional electrons onto the substrate can be generated by EFR.

IV. EFR with Ar/O_2 Gas Mixtures

The addition of oxygen to the argon gas mixture enables the generation of negative ions and the transition of the electropositive Ar discharge to an electronegative plasma. The densities of Ar^+, O_2^+, O^- and electrons, as well as the discharge electronegativity are shown in Fig. 5 as a function of the O_2 mole fraction in the inlet flow for otherwise the base-case conditions with φ = 0°. The electronegativity is the ratio of densities of $[O^-]/[e]$. Through dominantly dissociative electron attachment of O_2 to form O^-, the electron density decreases with increasing O_2 inflow while that of O^- increases. At 50% O_2, the total negative charge in the plasma bulk is nearly equally due to O^- and electrons. The total positive ion density decreases from 2×10^{10} cm^{-3}, for the pure Ar discharge to 1.4×10^{10} cm^{-3} at 50% O_2, a consequence of more power being dissipated in non-ionizing collisions with the increase in O_2 fraction. The total discharge electronegativity increses from to 1.05 at 50% O_2.

Due to the change in electron density and the subsequent changes in power deposition, the DC self-bias is a sensitive function of the Ar/O_2 ratio. V_{dc} as a function of the voltage phase angle φ for Ar/O_2 ratios of 100/0, 90/10, 75/25 and 50/50 is shown in Fig. 6a. The general trend of decreasing magnitude of V_{dc} (less negative) with increasing phase angle φ occurs for all gas mixtures. This trend is a result of the EAE.

A second major trend is an increase of the magnitude of V_{dc} (more negative) with increasing O_2 mole fraction. Due to the electronegativity of O_2 containing plasmas and dissipation of power in non-ionizing collisions with O_2, increasing the mole fraction of O_2 requires higher applied voltages to maintain a constant power deposition. The total voltage amplitude V_0 as a function of the phase angle φ for different Ar/O_2 ratios is shown in Fig. 6b. At φ = 0°, V_0 increases by approximately 18% from 1300 V with Ar/O_2 = 100/0 to 1545 V at Ar/O_2 = 50/50. For a given electrical or geometrical asymmetry V_{dc} is proportional to V_0, and so on this basis alone, the magnitude of the V_{dc} should increase (become more negative) with increasing O_2 mole

fraction.

The axial component of the electric field between the two electrodes, $E_z(z, t)$, radially averaged across the wafer is shown in Fig. 7. Each column represents a constant phase angle with φ = 0°, 45°, 90°, 135° and 180°. Each row in turn represents cases at constant gas ratio and varying phase angle with for Ar/O_2 = 100/0 (Fig. 7a), 90/10 (Fig. 7b), 75/25 (Fig. 7c) and 50/50 (Fig. 7d). The voltage waveforms are shown in the bottom row (Fig. 7e). The dotted line in the images is the $E_z(z, t) = 0$ contour.

The magnitude of the EFR increases with increasing oxygen mole fraction for all phase angles φ. The EFR has a peak magnitude of 47 V/cm (E/N = 3650 Td, 1 Td = 10^{-17} V-cm^2) in the absence of oxygen for φ =0, and a peak value of 94 V/cm (7300 Td) with Ar/O_2 = 50/50 while the EFR extends deeper into the plasma. In pure argon, the sheath thickness during the cathodic phase is 9.5 mm and the extent of the EFR from the substrate during the anodic phase is 6 mm. For Ar/O_2 = 50/50, the sheath thickness is 15 mm and the extent of the EFR is 12 mm. Due to the lower applied sinusoidal voltage no electric field reversal occurs at the top electrode. In general, EFR occurs when electron transport to the surface has a limited time window during the anodic portion of the RF cycle or is impeded by other means. Since mobility μ_i is inversely proportional to mass and the generation of negative O^- ions produces a decrease in the electron density, the average mobility of negative charge carriers decreases. This decrease in mobility then requires a larger extracting electric field in the form of the EFR. With increase in O_2 fraction from zero to 50%, the electron density decreases to about 40% of that in pure argon. With the sum of the positive ion fluxes decreasing to 80% of their values with pure argon, the EFR increases by a factor of 2 (47 V/cm to 94 V/cm) to extract the needed electron current.

As with the pure argon base cases, the magnitude of the EFR decreases with increasing phase angle for all Ar/O_2 gas mixtures. The temporal modulation of the zero electric field contour in the bulk plasma also varies with phase angle. This modulation indicates that the effects of the VWT are not limited to the sheath, and could be responsible for small modulation that occurs in electron temperature. To some degree, this modulation is required by current continuity. Displacement current through the sheath is proportional to dE/dt – current which must be matched largely by conduction current in the bulk plasma. As dE/dt in the sheath varies with phase angle, there must be variation in conduction current in the bulk plasma which in turn requires modulation in the bulk electric field. The modulation of the E=0 contour is more pro-

nounced at higher Ar/O_2 ratios, indicating that the changes to the sheath potential structure (leading to more displacement current) which increase with the O_2 content extend beyond the immediate sheath region to modulate conduction current in the bulk plasma.

The time dependent densities of Ar^+, O^- and electrons are shown in Fig. 8 for $\varphi = 0°$ and $Ar/O_2 = 50/50$. Due to their low mobility and their being trapped in the positive plasma potential, the O^- ions (Fig. 8b) do not follow the modulated sheath and are confined to the bulk plasma at all times. There is some perturbation of the O^- density at the peak of the cathodic cycle at the top electrode, however the negative ions do not significantly contribute to the transport of negative charge to the surface. In contrast to the stationary O^- density profiles, the electron density profile, shown in Fig 8c, responds quickly to the applied potential. The electrons are confined to the plasma bulk during most of the RF period and only extend to the surface at the time of sheath collapse at 0.5 μs. As a result of this discrepancy in dynamic behavior between electrons and O^-, increasing the mole fraction of O^- in the system effectively reduces the transport of negative charges to the surface, thereby necessitating a larger EFR during the portion of the RF cycle during which there is sheath collapse.

With an increase of the magnitude of the DC self-bias V_{dc} and the applied voltage $V_{0,}$ the sheath potential and sheath width increase. The maximum width of the sheath increases from approximately 9 mm for pure argon to 15 mm for $Ar/O_2 = 50/50$. This increase in sheath width increases collisionality (reducing electron mobility) and increases the distance electrons need to traverse during the sheath collapse in order to reach the surface. Both effects limit electron transport and increase the need for and magnitude of the EFR.

These two mechanisms (the reduction in the density of mobile charge carriers by the increasing negative ion density and the confinement of electrons by the applied tailored voltage waveform) at least partially add, thereby increasing the magnitude and extent of spatial penetration of the EFR. Comparing the electric field configurations over the range of phase angles reveals a strong dependence of the EFR on gas mixture. With $Ar/O_2 = 50/50$, the magnitude of the EFR decreases with increasing phase angle – decreasing from 94 V/cm at $\varphi = 0°$ to 11 V/cm at $\varphi = 180°$, a total change of 83 V/cm. For the same phase angle shift for the pure argon plasma, the change in magnitude of the EFR is only 11 V/cm.

The interaction between the two mechanisms producing EFR also results in enhanced electron acceleration towards the wafer. The electron EADs incident onto the wafer are shown

in Fig. 9 for $\varphi = 0°$ (maximum EFR) and for $\varphi = 180°$ (minimum EFR) for different Ar/O_2 feedstock mixtures. With $\varphi = 180°$, the EFR is nominal, resulting in the electron EADs being largely thermal with average energies < 10 eV for bulk electron temperatures of 3.2 – 3.5 eV. There is a small increase in incident electron energy and narrowing of angular distribution for Ar/O_2 = 50/50 where the magnitude of the EFR begins to increase. With $\varphi = 180°$ when most of the negative charge is carried by heavy O^- ions, electron transport is still sufficient to balance positive ion transport due to the sheath being collapsed during most of the RF cycle. There is little additional electron acceleration by an EFR necessary to balance the positive ion flux.

With $\varphi = 0°$, the EFR is well established with peak magnitudes reaching nearly 100 V/cm for Ar/O_2 = 50/50. The maximum electron energy incident onto the wafer extends from 30 eV for pure argon to 100 eV for Ar/O_2 = 50/50. The angular distribution narrows from ±45 degrees for pure argon to a ±20 degree spread for Ar/O_2 = 50/50. The wide range of electron energy, while the minimum energy is nearly constant for oxygen containing mixtures, suggests that the electron attracting sheath is the equivalent of the thin-sheath-limit for accelerating ions into the electrode. That is, the electron transit time across the sheath is short compared to the RF period, and so electrons are accelerated to the instantaneous sheath potential. The lower energy component of the EAD is likely sustained by continuing thermalization of electrons through collisions inside the sheath.

The mean electron energies at the wafer surface as a function of the phase angle, $\bar{\varepsilon}(\varphi)$, for different Ar/O_2 mixtures are shown in Fig. 10a. As with the EADs, the trends correlate with the magnitude and depth into the plasma of the EFR. Mean energies for $\varphi = 180°$ have a nominal dependence on gas mixture, extending from 6.2 eV for pure argon to 9.7 eV for Ar/O_2 = 50/50. Although this is a change of a factor of 1.5, the absolute change is only 3.5 eV. Mean energies for $\varphi = 0°$ extend from 16.7 eV for pure argon to 57.7 eV for Ar/O_2 = 50/50, an increase by a factor of 3.4 and absolute change of 41 eV. The same mechanisms producing a decrease in mean energy produces a decrease in the mean angle with which electrons strike the waver, as shown in Fig. 10b as a function of the phase angle and gas mixture. For a given Ar/O_2 mixture, the mean angle increases with increasing φ. As with the mean energy, these changes are most pronounced at the highest oxygen content. For Ar/O_2 = 50/50 the mean angle increases from 6.4° at $\varphi = 0°$ to 20.3° at $\varphi = 180°$, a 3-fold increase.

V. Concluding Remarks

The use of voltage waveform tailoring (VWT) to generate and control electric field reversals (EFRs) during the sheath collapse in low pressure capacitively coupled RF plasmas sustained in Ar/O_2 mixtures was computationally investigated. The purpose of this investigation is to assess the potential of this technique to accelerate electrons into sub-micron HAR etch features to compensate positive surface charging inside these structures. The effects of the Ar/O_2 feed gas ratio as well as voltage waveforms on the electron energy-angular distributions (EAD) incident onto the wafer surface were investigated while keeping the power deposition constant, as would be the practice in industry. To maintain the plasma density and reduce its dependence on the voltage waveform, a high frequency RF voltage was applied to the top electrode. The substrate bias waveform consisted of a sinusoidal signal and its first 4 harmonics with the even harmonics having a variable phase shift φ. The strength of the EFR increases with the O_2 mole fraction and with a decrease in φ. The correlation with the O_2 mole fraction is a consequence of the electronegative nature of the oxygen. The increase in O_2 mode fraction reduces the electron density while increasing negative ion density, which results in a decrease in the average negative charge carrier mobility. To maintain constant power, a larger applied voltage is required.

The consequences of the phase angle on EFR can be attributed to two major effects: i) the electrical asymmetry effect is maximum at $\varphi = 0°$ ("peak" waveform), leading to a large DC self-bias (most negative) and thick sheath and ii) the time that the sheath collapses is minimized at $\varphi = 0°$ and maximized at $\varphi = 180°$. Both of these effects enhance the EFR. Since the ion flux to the substrate must be balanced by electrons on a time average while electron transport to the substrate by diffusion is insufficient to do so in the presence of these transport limiting factors.

For a fundamental driving frequency of 1 MHz and a power of 1 kW applied to substrate, the bias waveform enable significant control of the electron energy and angle distributions onto the wafer surface. The relative and absolute changes in mean electron energy were a strong functions of the Ar/O_2 feed gas ratio and most pronounced in the Ar/O_2 =50/50 mixture, while being significant in all configurations that were investigated. The fact that electronegative gases increases the magnitude of the EFR, and its ability to accelerate electrons into the wafer, suggests that process gas compositions used in semiconductor plasma etching processes, which often contain strongly electronegative species, can potentially profit from this mechanism as well.

The details of plasma etching processes critically depend on the ion energy and angular

distributions onto the wafer. Although VWT is able to control the electron EADs onto the wafer, this cannot be done independently of also changing the ion EADs. Changes in the VWT configuration changes the DC bias which translates into changing the average ion energy onto the wafer. The shape of the ion EAD will depend on number of harmonics and the phase angle. Nevertheless, some of the scaling of the EAD described in this work could allow for favorable synergies with current trends in semiconductor manufacturing. Higher applied voltages, as used in plasma etching of HAR features, combined with a voltage waveform resembling the peak-waveform, will produce high energy, narrow angle fluxes of electrons into the wafer surfaces. These fluxes have the properties required to address intra-feature charging.

To evaluate the efficacy of VWT in the context of actual plasma etching processes, it is important to investigate relevant process conditions using halogen containing gas mixtures combined with feature scale simulations that include the effects of the electron and ion EADs on charge accumulation, feature deformation and depth limited etch rates. There are still open questions with respect to the feasibility of plasmas sustained by complex waveforms at very high powers and the technical difficulties related to power matching, filtering, phase locking and metrology as well as economic considerations.

Due to its potential versatility, future implementations of VWT may be not limited to conventional CCPs but could find application in different contexts such as in inductively coupled plasmas. These applications could be for similar surface charge remediation on biased electrodes or the prevention of material erosion near the antennas caused by high energy ions in E-mode operation during pulsed operation. A broader set of waveform configurations should be investigated as the physical mechanisms discussed here are, in principle, not dependent on any specific waveform. These investigations may include the use of non-consecutive harmonics, pulsed higher harmonics, transient phase shifts or entirely non harmonic waveforms.

Data Availability

The data that support the findings of this study are available from the corresponding author upon reasonable request.

Acknowledgements

This work was supported by Samsung Electronics Ltd. and the National Science Foundation **(**PHY-2009219**)**. These results were also based upon work supported by the U.S. Department of Energy, Office of Science, Office of Fusion Energy Sciences under award numbers and DE-SC0020232 and DE-SC0001939.

References

[1] V. M. Donnelly and A. Kornblit, J. Vac. Sci. Technol. A Vacuum, Surfaces, Film. **31,** 050825 (2013).

[2] H. Tanaka, M. Kido, K. Yahashi, M. Oomura, R. Katsumata, M. Kito, Y. Fukuzumi, M. Sato, Y. Nagata, Y. Matsuoka, Y. Iwata, H. Aochi and A. Nitayama, Dig. Tech. Pap. - Symp. VLSI Technol. 14 (2007).

[3] Y. Li, IEEE Solid-State Circuits Mag. **12,** 56 (2020).

[4] B. Wu, A. Kumar and S. Pamarthy, Journal of Applied Physics **108,** 51101 (2010).

[5] S. Rauf and A. Balakrishna, J. Vac. Sci. Technol. A Vacuum, Surfaces, Film. **35,** 021308 (2017).

[6] G. Le Dain, A. Rhallabi, C. Cardinaud, A. Girard, M.-C. Fernandez, M. Boufnichel and F. Roqueta, J. Vac. Sci. Technol. A **36,** 03E109 (2018).

[7] J. C. Wang, W. Tian, S. Rauf, S. Sadighi, J. Kenney, P. Stout, V. S. Vidyarthi, J. Guo, T. Zhou, K. Delfin, N. Lundy, S. C. Pandey, S. Guo and G. S. Sandhu, Plasma Sources Sci. Technol. **27,** 94003 (2018).

[8] B. Radjenović and M. Radmilović-Radjenović, Engineering **06,** 1 (2014).

[9] C. Han, Z. Wu, C. Yang, L. Xie, B. Xu, L. Liu, Z. Yin, L. Jin and Z. Huo, Semicond. Sci. Technol. **35,** 045003 (2020).

[10] B. M. Radjenović, M. D. Radmilović-Radjenović and Z. L. Petrović, IEEE Trans. Plasma Sci. **36,** 874 (2008).

[11] H. Jansen, M. De Boer, R. Wiegerink, N. Tas, E. Smulders, C. Neagu and M. Elwenspoek, Microelectron. Eng. **35,** 45 (1997).

[12] R. J. Belen, S. Gomez, M. Kiehlbauch and E. S. Aydil, J. Vac. Sci. Technol. A Vacuum, Surfaces, Film. **24,** 350 (2006).

[13] N. Negishi, M. Miyake, K. Yokogawa, M. Oyama, T. Kanekiyo and M. Izawa, J. Vac. Sci. Technol. B, Nanotechnol. Microelectron. Mater. Process. Meas. Phenom. **35,** 051205 (2017).

[14] G. S. Hwang, J. Vac. Sci. Technol. B Microelectron. Nanom. Struct. **15,** 70 (1997).

[15] T. Nozawa, T. Kinoshita, T. Nishizuka, A. Narai, T. Inoue and A. Nakaue, Jpn. J. Appl. Phys. **34,** 2107 (1995).

[16] D. Zhang, S. Rauf and T. Sparks, IEEE Trans. Plasma Sci. **30,** 114 (2002).

[17] A. Agarwal, S. Rauf and K. Collins, J. Appl. Phys. **112,** 33303 (2012).

[18] P. Hartmann, L. Wang, K. Nösges, B. Berger, S. Wilczek, R. P. Brinkmann, T. Mussenbrock, Z. Juhasz, Z. Donkó, A. Derzsi, E. Lee and J. Schulze, J. Phys. D. Appl. Phys. **54,** 255202 (2021).

[19] U. Czarnetzki, D. Luggenhölscher and H. F. Döbele, Plasma Sources Sci. Technol. **8,** 230 (1999).

[20] Y. X. Liu, Q. Z. Zhang, J. Liu, Y. H. Song, A. Bogaerts and Y. N. Wang, Appl. Phys. Lett. **101,** 114101 (2012).

[21] S. Sharma and M. M. Turner, J. Phys. D. Appl. Phys. **47,** 285201 (2014).

[22] S. Brandt, B. Berger, Z. Donkó, A. Derzsi, E. Schüngel, M. Koepke and J. Schulze, Plasma Sources Sci. Technol. **28,** 095021 (2019).

[23] J. Schulze, E. Schüngel, Z. Donkó and U. Czarnetzki, Plasma Sources Sci. Technol. **20,** 15017 (2011).

[24] Z. Donkó, A. Derzsi, M. Vass, J. Schulze, E. Schuengel and S. Hamaguchi, Plasma Sources Sci. Technol. **27,** 104008 (2018).

[25] S. Brandt, B. Berger, E. Schüngel, I. Korolov, A. Derzsi, B. Bruneau, E. Johnson, T. Lafleur, D. O'Connell, M. Koepke, T. Gans, J. P. Booth, Z. Donkó and J. Schulze, Plasma Sources Sci. Technol. **25,** 17 (2016).

[26] B. G. Heil, U. Czarnetzki, R. P. Brinkmann and T. Mussenbrock, J. Phys. D. Appl. Phys. **41,** 165202 (2008).

[27] T. Lafleur, Plasma Sources Sci. Technol. **25,** 013001 (2015).

[28] A. Derzsi, T. Lafleur, J. P. Booth, I. Korolov and Z. Donkó, Plasma Sources Sci. Technol. **25,** 15004 (2015).

[29] G. A. Skarphedinsson and J. T. Gudmundsson, Plasma Sources Sci. Technol. **29,** 084004 (2020).

[30] M. J. Kushner, Journal of Physics D: Applied Physics **42,** 194013 (2009).

[31] P. Tian and M. J. Kushner, Plasma Sources Sci. Technol. **24,** 34017 (2015).

[32] S. Huang, C. Huard, S. Shim, S. K. Nam, I.-C. Song, S. Lu and M. J. Kushner, J. Vac. Sci. Technol. A **37,** 031304 (2019).

[33] D. S. Stafford and M. J. Kushner, J. Appl. Phys. **96,** (2004).

[34] U. Czarnetzki, J. Schulze, E. Schüngel and Z. Donkó, Plasma Sources Sci. Technol. **20,** (2011).

[35] J. Schulze, Z. Donkó, B. G. Heil, D. Luggenhölscher, T. Mussenbrock, R. P. Brinkmann and U. Czarnetzki, J. Phys. D. Appl. Phys. **41,** 105214 (2008).

[36] J. Schulze, E. Schüngel and U. Czarnetzki, J. Phys. D. Appl. Phys. **42,** 092005 (2009).

Figures Captions

1. Geometry and circuit used in the model. a) Schematic of the dual frequency capacitively coupled plasma reactor used in this investigation. b) Equivalent circuit diagram of the reactor. Source power at 80 MHz is applied to the top electrode. The 1 MHz tailored waveform is applied to the bottom electrode.
2. Plasma properties as a function of phase angle φ for the pure argon plasma with a constant high frequency power of 100 W and constant bias power of 1 kW. a) Applied voltage amplitudes for the high frequency source (V_{hf}) and amplitude of the low frequency bias (V_o). top and bottom electrode. b) DC self-bias.
3. Plasma properties for the pure argon plasma averaged across the wafer as a function of height above the wafer and time during the low frequency,1 MHz cycle. Values are shown (left-to-right) for phase angles of φ = 0, 45, 90, 135, 180°. a) Axial component of the electric field, b) Ar^+ density, c) electron density and d) applied voltage waveform on the substrate. The Ar^+ and electron densities are plotted on a log-scale spanning 2 decades with the maximum value noted in each image.
4. Properties of electrons incident onto the wafer for the pure argon plasma. a) Electron energy and angular distributions for different phase angles plotted on a log-scale spanning 2 decades. b) Mean electron energy and mean electron angle of incidence as a function of phase angles.
5. Spatially averaged densities of Ar^+, e^-, O_2^+ and O^-, and electronegativity of Ar/O_2 plasmas as a function of the O_2 mole fraction with a phase angle of φ = 0°.
6. Plasma properties as a function of phase shift φ for different Ar/O_2 ratios when keeping source and bias powers constant. a) DC self-bias produced on the powered substrate. b) Applied voltage amplitude V_o.
7. Radial average of the vertical component of the electric field as a function of time during a single 1 MHz cycle and distance from bottom electrode different gas mixtures. Ar/O_2 = a) 100/0, b) 90/10, c) 75/25, d) 50/50. e) Normalized applied voltage V_0. Results are shown for phase shifts of (left-to-right columns) φ = 0, 45, 90, 135 and 180° The dotted line is for E = 0, the separation between negative electric fields pointing down and positive pointing up.
8. Plasma properties for Ar/O_2 = 50/50 and a phase shift of φ = 0°. a) Radial average of the Ar^+ density as a function of time during a single 1 MHz RF cycle plotted on a log-scale over 2-

decades. b) O^- density (log-scale, 2-decades) and c) electron density (log-scale 3-decades). The maximum density is noted in each image. d) e) Normalized voltage amplitude V_0

9. Electron energy and angular distributions incident onto the wafer surface for different Ar/O_2 ratios plotted on a log-scale over 2 decades with phase shifts of a) $\varphi = 0°$ and b) $\varphi = 180°$. The EAD increases in energy and narrows in angle with increasing O_2 fraction, an effect that is most prominent for a) $\varphi = 0°$.
10. Properties of the electron velocity distribution incident onto the wafer for different Ar/O_2 ratios as a function of phase shifts φ. a) Mean electron energy and b) mean angle of incidence. Decreasing phase angle increases the incident electron energy and narrows the angular distribution, with the effect being most prominent for large O_2 mole fractions.

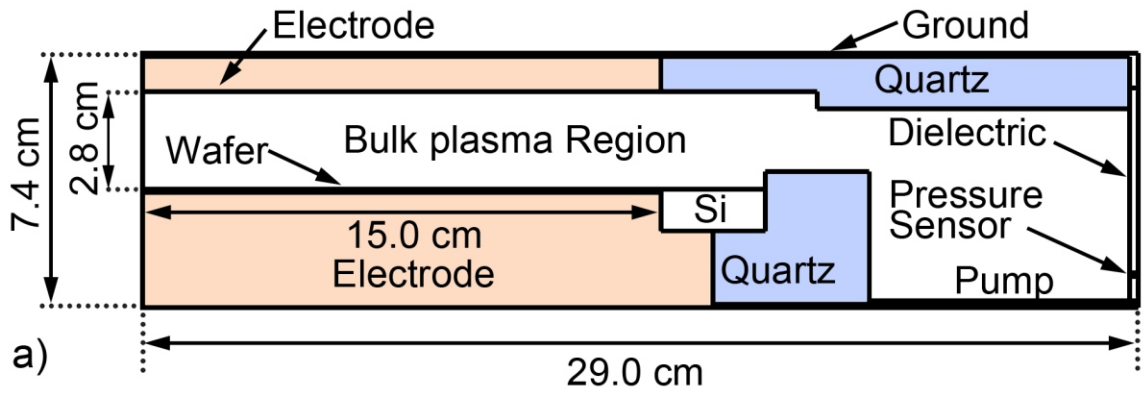
Electrode
Ground
Quartz
Dielectric
Wafer
Bulk plasma Region
Si
Pressure
Sensor
15.0 cm
Electrode
Quartz
Pump
7.4 cm
2.8 cm
29.0 cm

a)

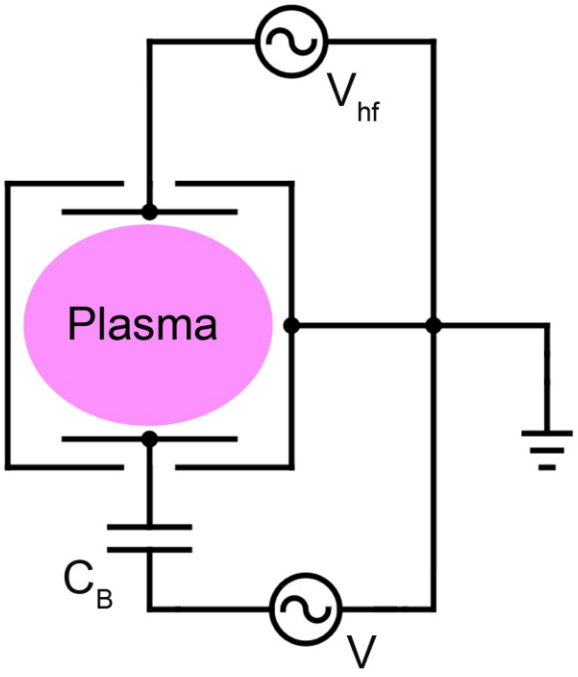
V_{hf}
Plasma
C_B
V

b)

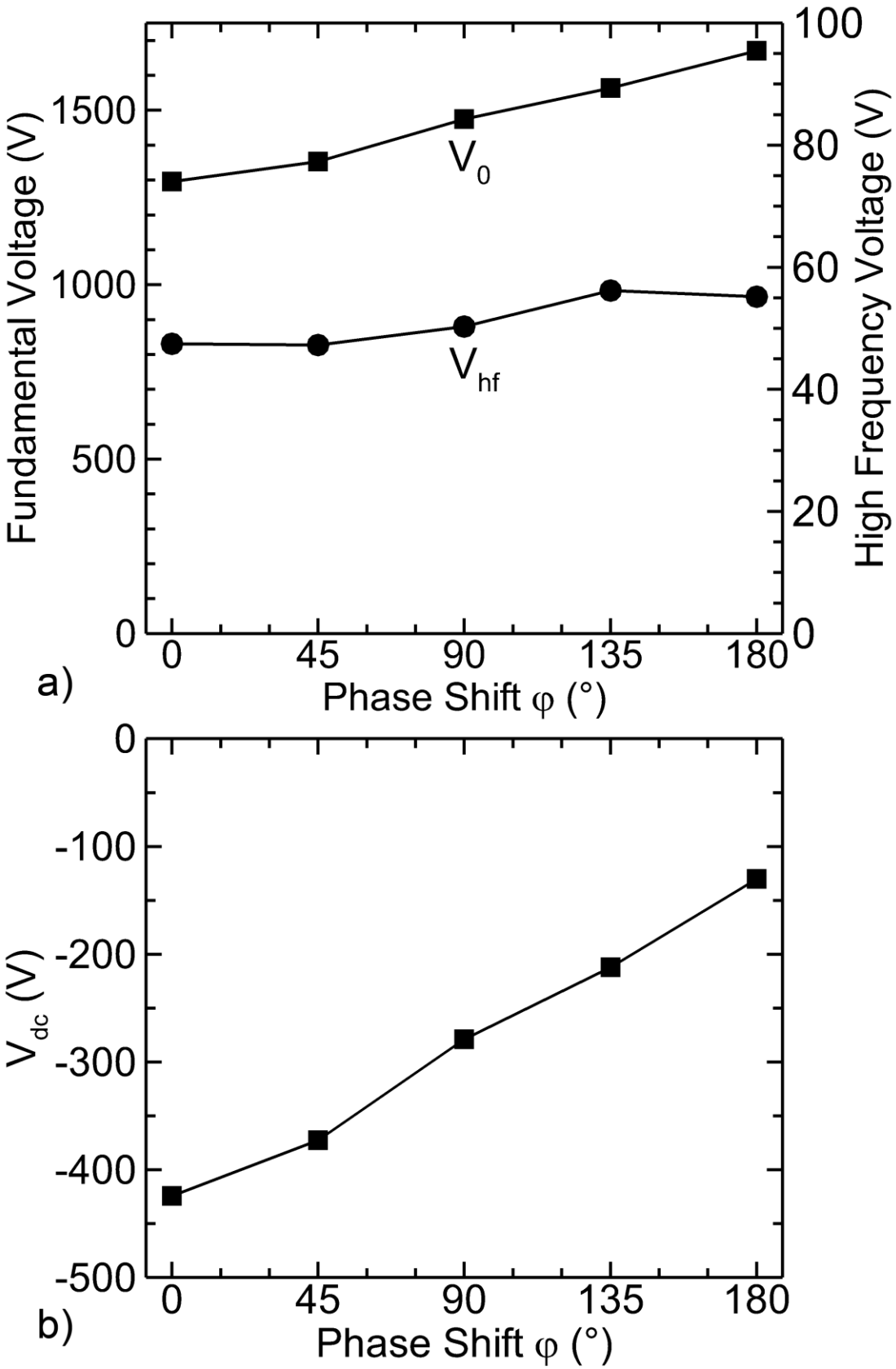

Kruger et al.
Fig. 2 of 10

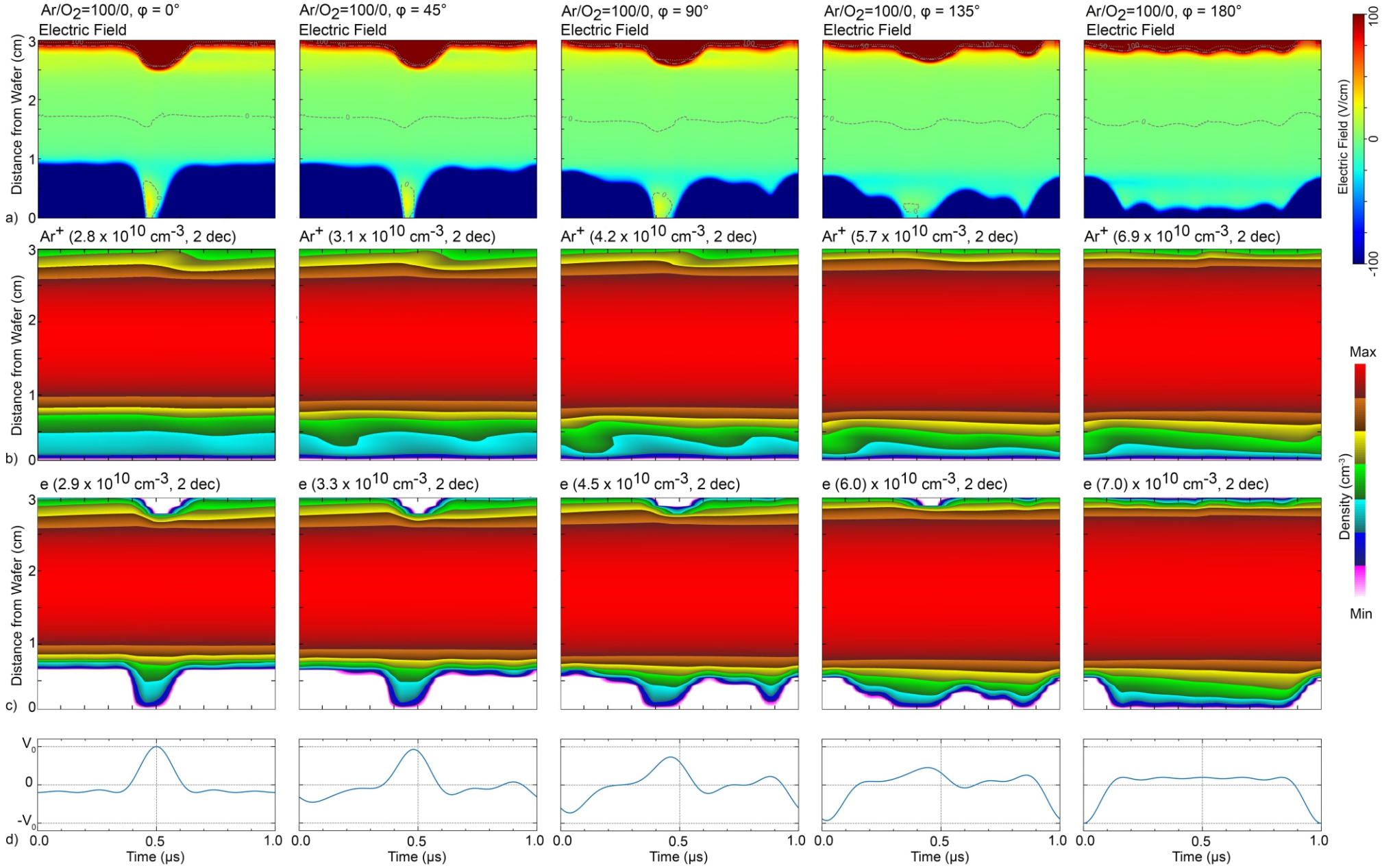

Kruger et al.
Fig. 3 of 10

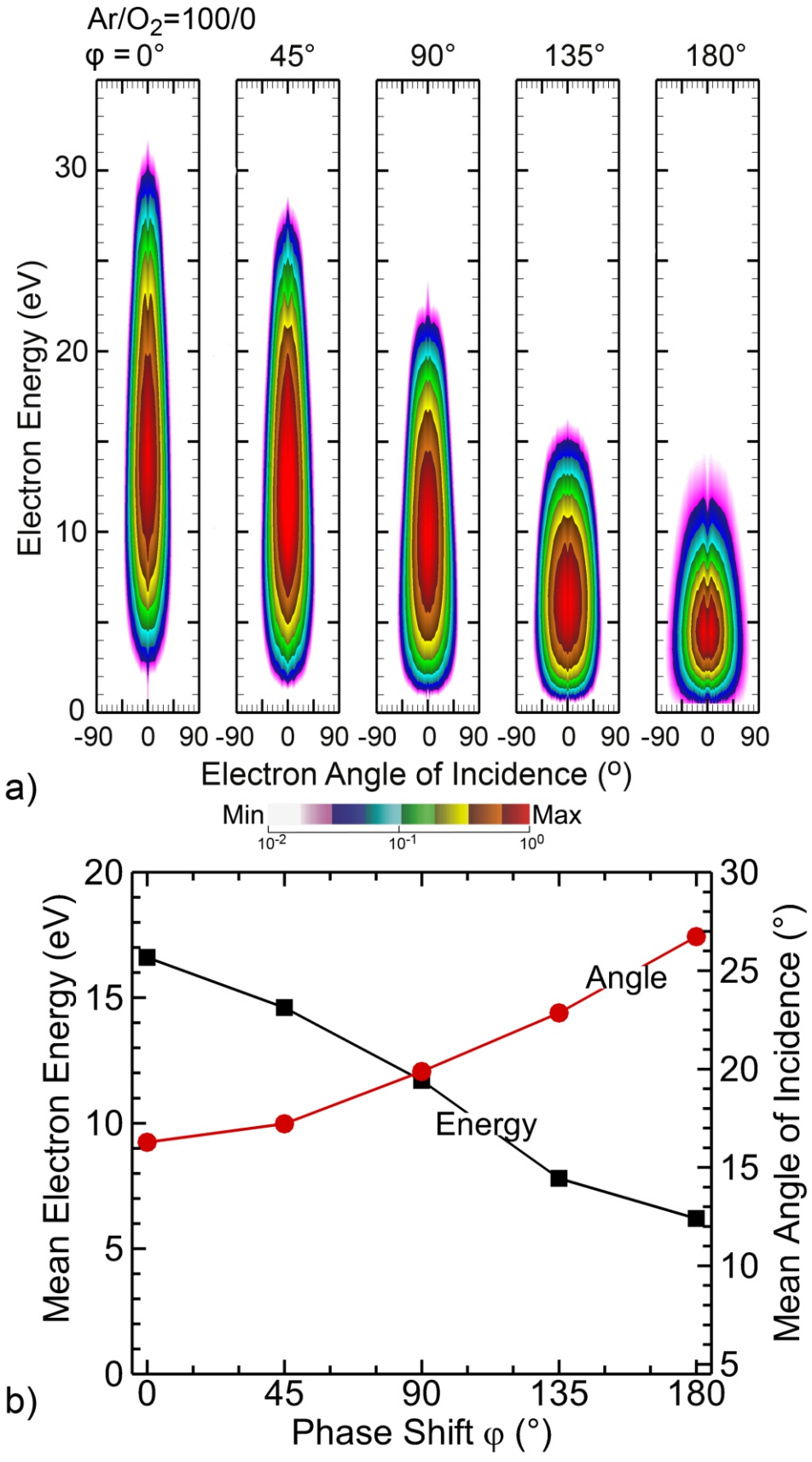

Kruger et al.
Fig. 4 of 10

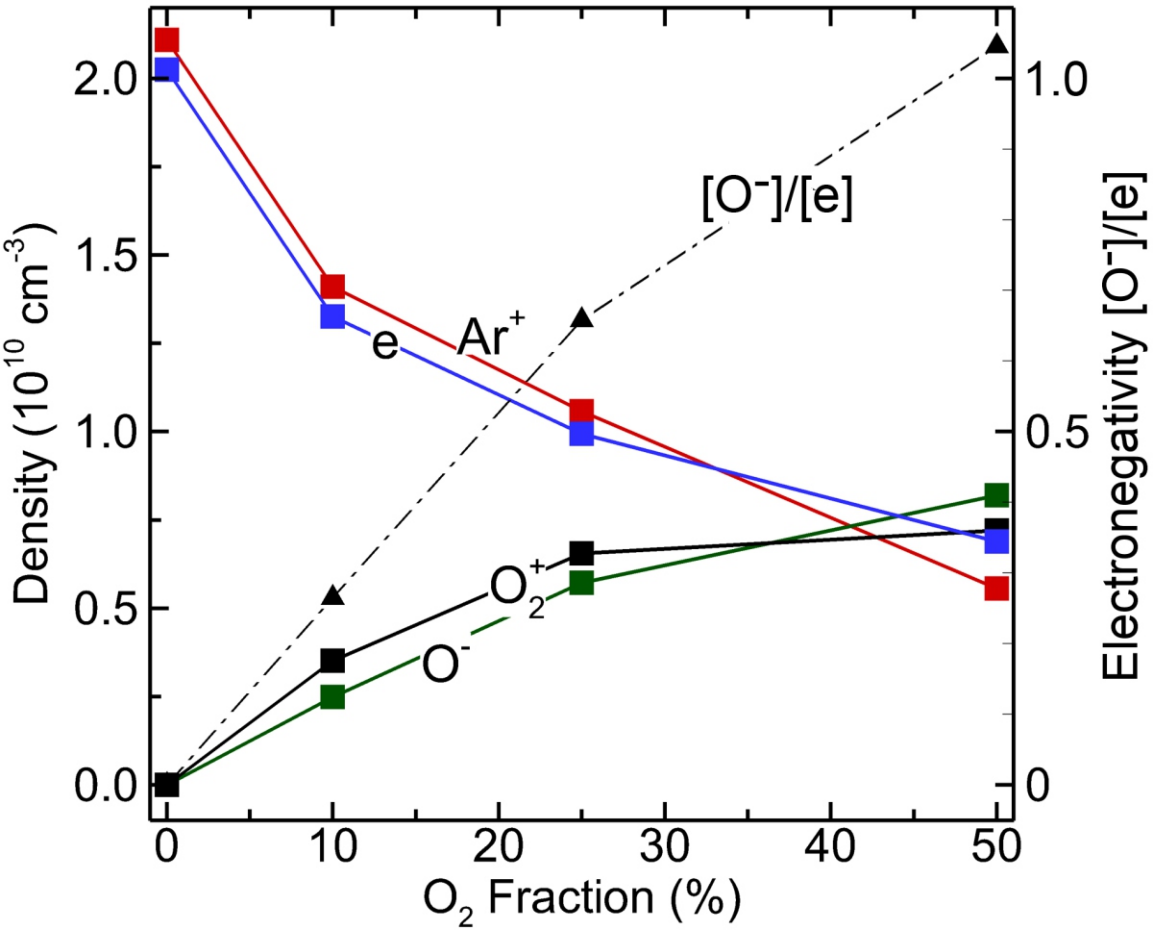

Kruger et al.
Fig. 5 of 10

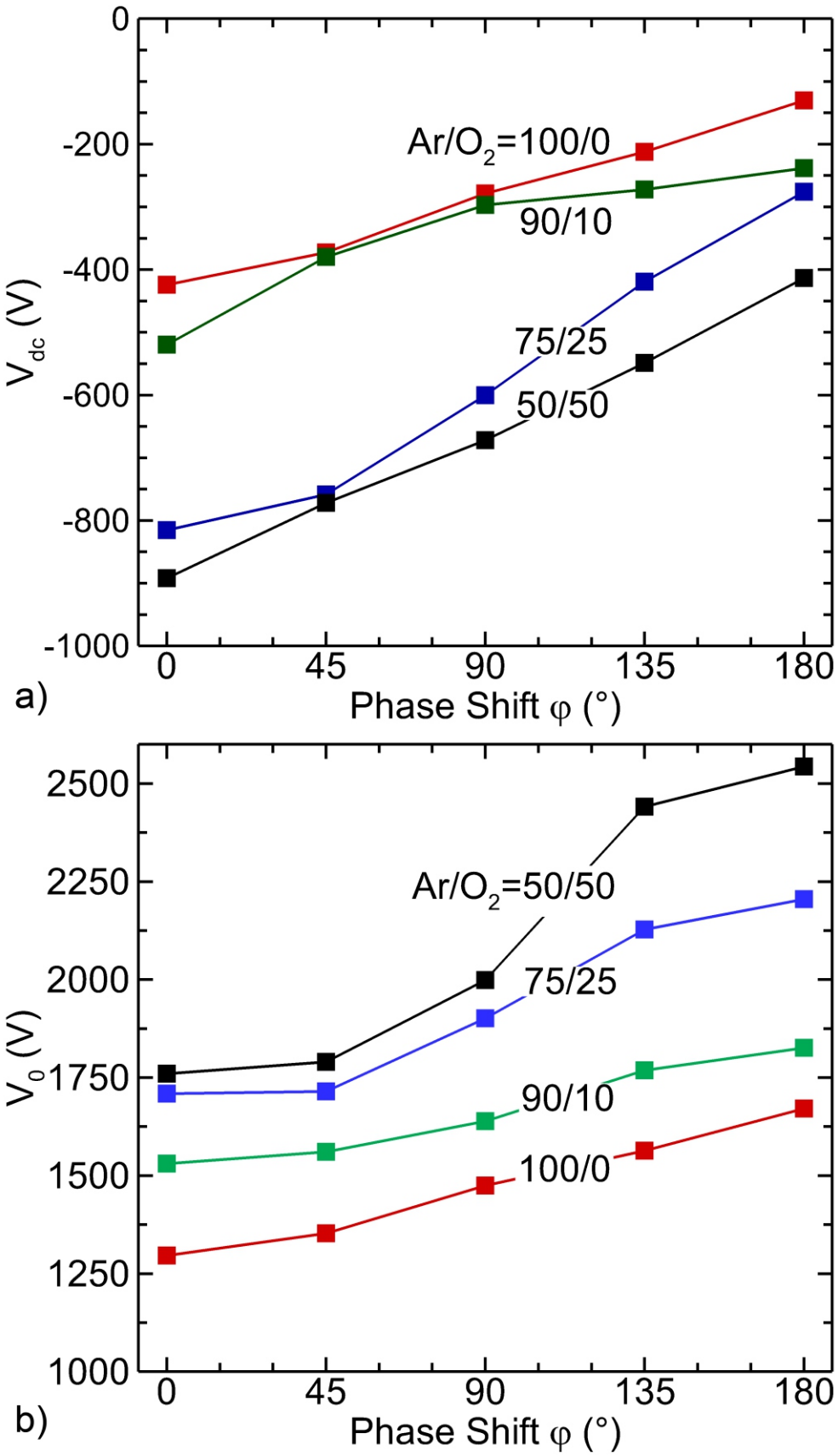

Kruger et al.
Fig. 6 of 10

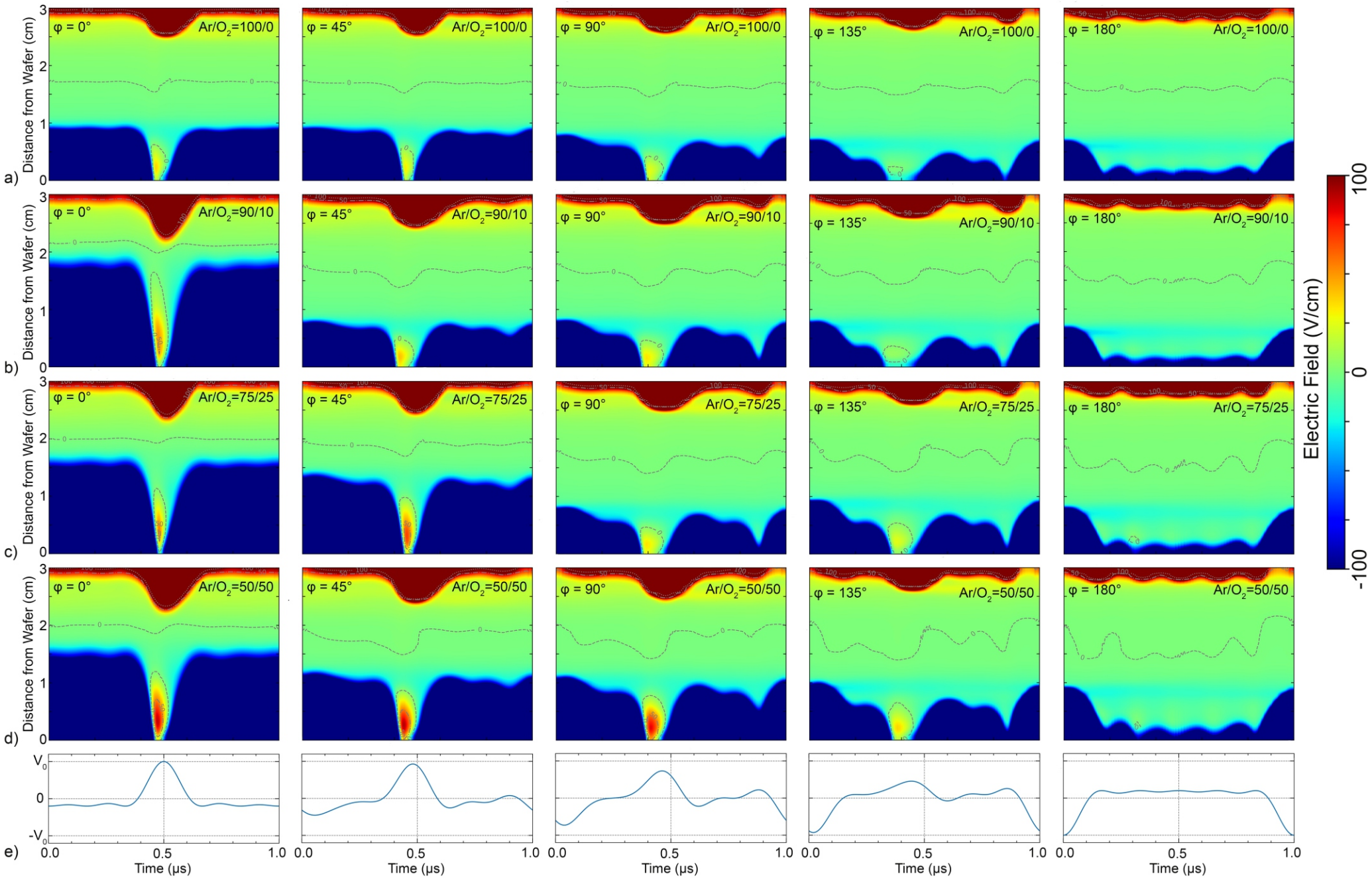

Kruger et al.
Fig. 7 of 10

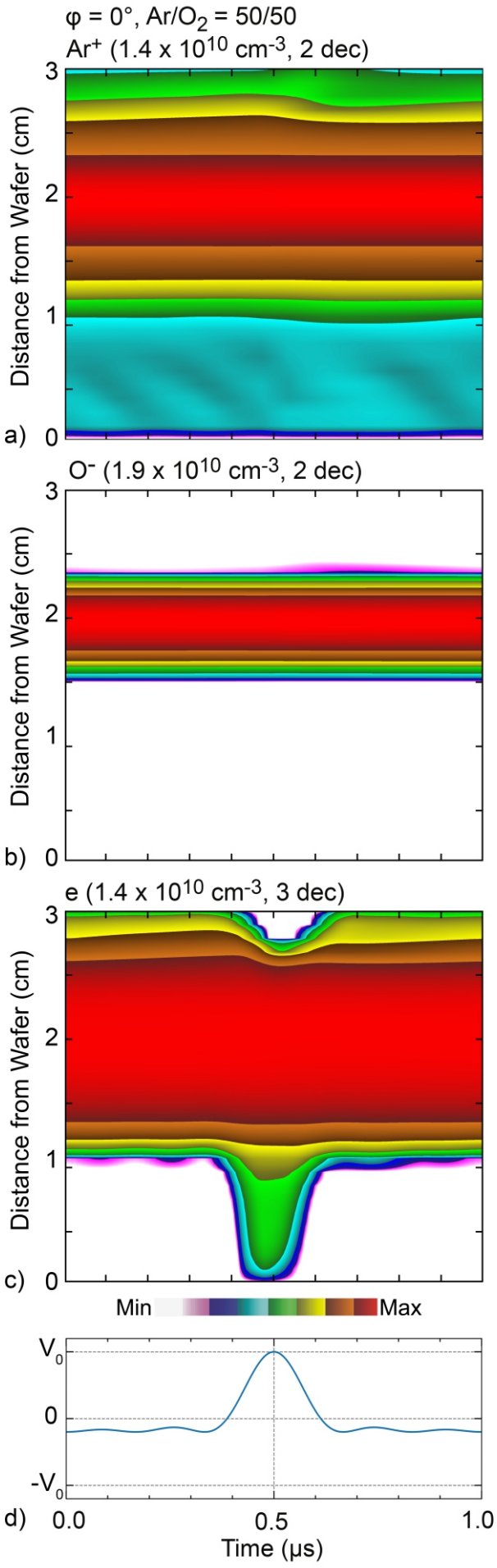

Kruger et al.
Fig. 8 of 10

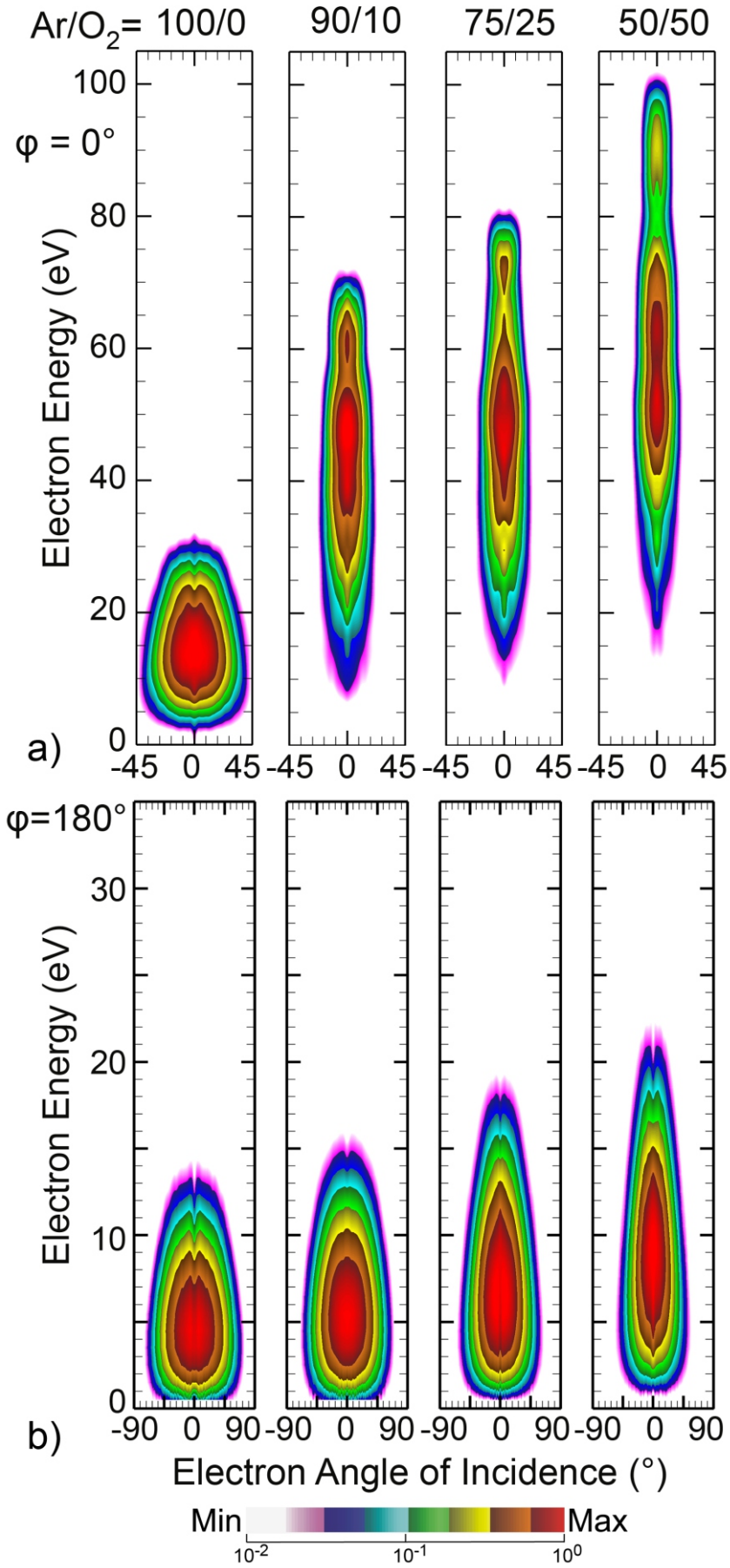

Kruger et al.
Fig. 9 of 10

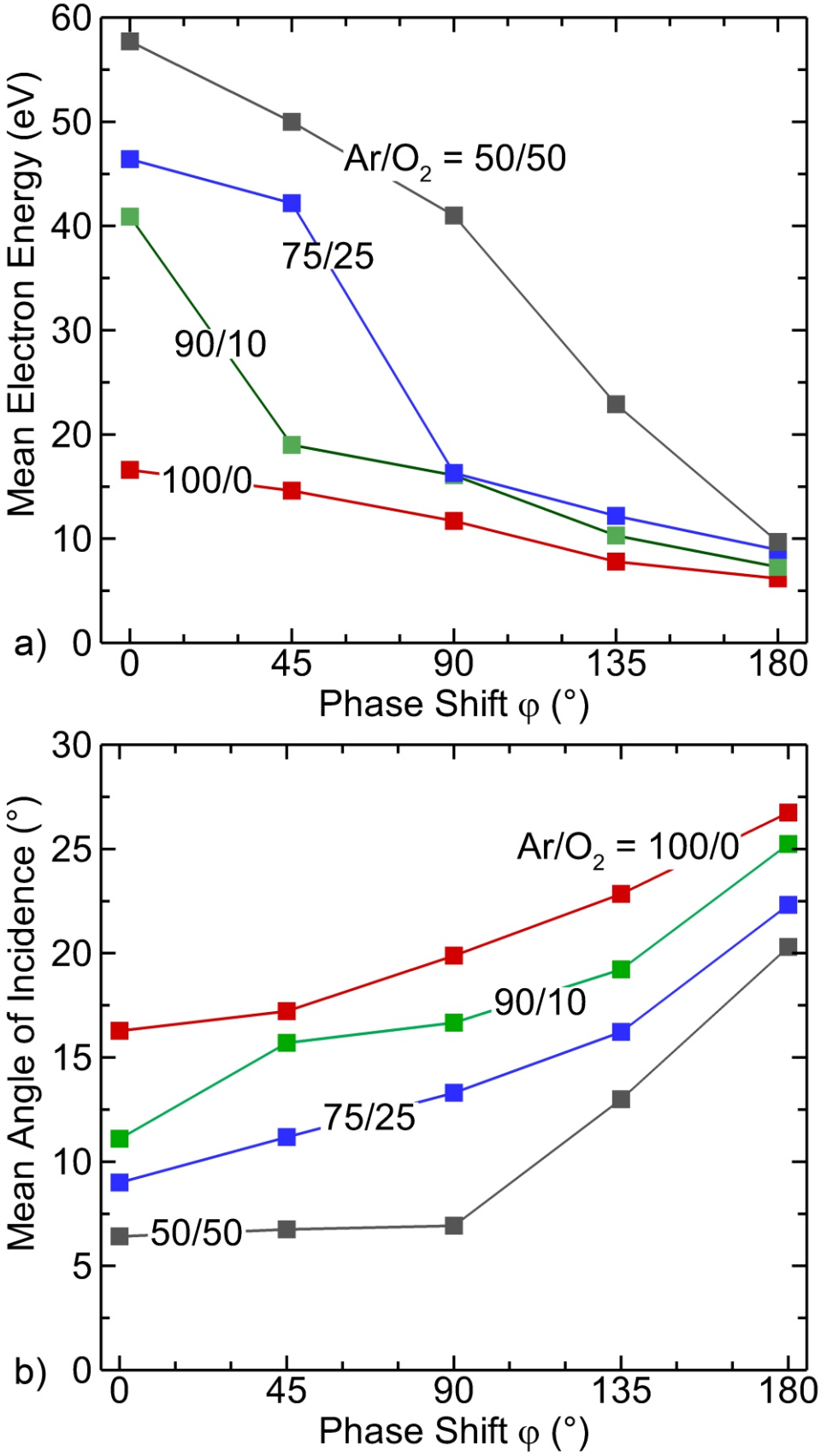

Kruger et al.
Fig. 10 of 10